Publication Year	2016
Acceptance in OA@INAF	2020-06-23T16:50:56Z
Title	Present-day aeolian activity in Herschel Crater, Mars
Authors	CARDINALE, MARCO; Silvestro, Simone; Vaz, David A.; Michaels, Timothy; Bourke, Mary C.; et al.
DOI	10.1016/j.icarus.2015.10.022
Handle	http://hdl.handle.net/20.500.12386/26202
Journal	ICARUS
Number	265

Elsevier Editorial System(tm) for Icarus
Manuscript Draft

Manuscript Number:

Title: Present-Day Aeolian Activity in Herschel Crater, Mars.

Article Type: Regular Article

Keywords: Sand transport; Dunes; Ripples, Aeolian Processes; Herschel Crater.

Corresponding Author: Dr. Marco Cardinale, Ph.D.

Corresponding Author's Institution: Università degli Studi G.d'Annunzio

First Author: Marco Cardinale, Ph.D.

Order of Authors: Marco Cardinale, Ph.D.; Simone Silvestro, Ph.D; David A. Vaz, Ph.D; Timothy Michaels, Ph.D; Goro Komatsu, Ph.D; Mary Bourke, Prof.; Lucia Marinangeli, Prof.

Abstract: In this report, we show evidence for ripple and dune migration in Herschel Crater on Mars. We estimate an average dune migration of 0.8 meters and a minimum ripple migration of 1.1 meters in a time span of 3.7 Earth-Years.

These dunes and ripples are mainly shaped by prevailing winds coming from the north, however we also report the presence of secondary winds enhanced by the crater rim at regional scale and deflected by the dune topography at the dune scale.

These last are predicted by the Mars Regional Atmospheric Modeling System (MRAMS), an atmospheric mesoscale model, while the dominant flows from the north are underestimated.

Modeled winds at the local scale refer that a multi directional wind regime is indicated as the first cause of the diverse set of ripples overlapping one on other.

For the first time, a survey integrating the assessment of dune and ripple migration is presented, showing how dune topography can influence the migration patterns of ripples and how underlying regional topography seems to control the rates of dune migration.

The migration patterns suggest that the prevailing winds from the north are locally-deflected winds (blowing from the NNW and from the NNE before deflection).

Suggested Reviewers: Matthew Choinacki
chojan1@pirl.lpl.arizona.edu

Candice Hansen
cjhansen@psi.edu

Robert A. Craddock
craddockb@si.edu

Rosalyn K. Hayward
rhayward@usgs.gov

Paul Geissler
pgeissler@usgs.gov

Opposed Reviewers:

Cover Letter

Editor
Editorial office of Icarus

May 08th, 2015

Dear Editor,We are submitting a manuscript entitled “Present-day aeolian activity in Herschel Crater, Mars.” prepared by M. Cardinale et al. to this journal
We would like to submit the manuscript only for the Online version and we would like to make colour choises for article’s 11figures as follows:

Online version
Colour: Figure 1, Figure 2, Figure 3, Figure 4, Figure 6, Figure 8, Figure 9, Figure 10, Figure 11, Figure 12.
B/W: Figure 5, Figure 7, Table 1, Table 2.

Sincerely yours,

Marco Cardinale

Marco Cardinale
Dipartimento di Scienze
Psicologiche della Salute e del Territorio
Universita' d'Annunzio
Via dei Vestini 31.
66013 Chieti, Italy
Phone: +39 – 0871- 3555331.
email: marco.cardinale@unich.it

Present-day aeolian activity in Herschel Crater, Mars.

Marco Cardinale[1], Simone Silvestro[2,3], David A. Vaz[4,5] , , Timothy Michaels[3], Goro Komatsu[6],
Mary C. Bourke[7], Lucia Marinangeli[1],

[1]Dipartimento di Scienze Psicologiche della Salute e della Terra, Università G. d' Annunzio
Via dei Vestini 31, 66013 Chieti Scalo, Italy

[2]INAF, Osservatorio Astronomico di Capodimonte,
Salita Moiariello 16, Napoli, Italy.

[3]Carl Sagan Center, SETI Institute
189 N. Bernardo Avenue, Suite 100 Mountain View, CA
94043, USA

[4]Centre for Earth and Space Research of the University of Coimbra,
Observatório Astronómico da Universidade de Coimbra,
Almas de Freire, 3040-004 Coimbra, Portugal.

[5]CERENA, Instituto Superior Técnico,
Av. Rovisco Pais, 1049-001 Lisboa, Portugal.

[6]International Research School of Planetary Sciences
Università G. d' Annunzio
Viale Pindaro, 42
65127 Pescara, Italy.

[7] Department of Geography, Trinity College Dublin,
Dublin, Ireland.

Submitted to Icarus
08 05, 2015
17 pages including text and captions
- 12 figures
2 tables

Corresponding author: Marco Cardinale
Dipartimento di Scienze Psicologiche Umanistiche e della Terra, Università d'Annunzio
Via dei Vestini 31, 66013 Chieti Scalo, Italy
Phone: +39-0871-355-5331
email: marco.cardinale@unich.it

Proposed running Title:
Aeolian activity in Herschel Crater (Mars).

Abstract

In this report, we show evidence for ripple and dune migration in Herschel Crater on Mars.

We estimate an average dune migration of 0.8 meters and a minimum ripple migration of 1.1 meters in a time span of 3.7 Earth-Years.

These dunes and ripples are mainly shaped by prevailing winds coming from the north, however we also report the presence of secondary winds enhanced by the crater rim at regional scale and deflected by the dune topography at the dune scale.

These last are predicted by the Mars Regional Atmospheric Modeling System (MRAMS), an atmospheric mesoscale model, while the dominant flows from the north are underestimated.

Modeled winds at the local scale refer that a multi directional wind regime is indicated as the first cause of the diverse set of ripples overlapping one on other.

For the first time, a survey integrating the assessment of dune and ripple migration is presented, showing how dune topography can influence the migration patterns of ripples and how underlying regional topography seems to control the rates of dune migration.

The migration patterns suggest that the prevailing winds from the north are locally-deflected winds (blowing from the NNW and from the NNE before deflection).

Keywords: Sand transport; Dunes; Ripples, Aeolian Processes; Herschel Crater.

1. Introduction and study area

The Martian surface has abundant active aeolian bedforms (Fenton, 2006; Bourke et al., 2008) which have been recently observed to migrate in the current climatic setting (Silvestro et al., 2010, 2011, 2013; Chojnacki et al., 2011; Hansen et al., 2011; Bridges et al., 2011, 2012, 2013; Geissler et al., 2013; Sparavigna, 2013). New techniques that take advantage of the high resolution of the HiRISE (High Resolution Imaging Science Experiment) data (McEwen et al., 2007) have been recently applied to characterize small-scale aeolian bedforms on Mars. The migration rates of ripples were computed using the Coregistration of Optically Sensed Images and Correlation (COSI-Corr) software (Bridges et al., 2012), while ripple trends were automatically derived using the Object-Based Ripple Analysis (OBRA) technique (Silvestro et al., 2011, 2013; Vaz and Silvestro, 2012, 2014).

The aim of this study is to use these two methods in combination to analyze dune and ripple patterns and migration using a pair of overlapping HiRISE images in Herschel Crater, a 300 km Noachian impact basin in the Mare Tyrrenium region (MC22) (Figure 1). The dunes of Herschel are of particular interest as they have been previously interpreted as ancient indurated aeolianites (due to the grooved pattern visible on the dune slopes; Malin and Edgett, 2000). More recent images from the HiRISE camera showed that such a pattern is formed by sand ripples which, together with the dunes, are consistently migrating (Bridges et al., 2007, 2011, 2013;).

However, first evidences for sand motion in the Herschel Crater have been detected by (Cardinale et al., 2012a).

In this work we compute ripple and dune migration rates and compare the migration directions with the present-day winds simulated by the Mars Regional Atmospheric Modeling System (MRAMS), a mesoscale atmospheric model (Michaels and Rafkin, 2008; Rafkin, 2001).

We use this wind model at two diverse grid scale to interpret the observed aeolian morphologies.

In this way, we test the capability of the wind model to predict the wind regime necessary for the creation and the evolution of the Herschel dune fields; we show that the aeolian activity that is shaping the dunes is not strictly unidirectional and that the topography of the crater is controlling the wind flow at the dune scale.

2. Methods

We conducted a detailed geomorphological analysis of dunes and ripples in Herschel Crater using a time series of HiRISE images and a stereo pair that was used to build a DTM with SOCET SET (Mattson et al., 2011) (Figure 1, Table 1). Images S1 and T3 (Table 1) were orthorectified over the DTM using the Co-registration of Optically Sensed Images and Correlation (COSI-Corr) software package (Leprince et al., 2007; Bridges et al., 2011). Dune morphometric parameters (slopes and aspect angles) were computed in ArcGIS and used to derive density stereoplots of the slipface surface vectors, providing an approximation to the main sediment flux direction (Figure 2d) (Silvestro et al., 2013). Ripple crestlines were mapped over the study dunes in the S1 image using the OBRA (Object-Based Ripple Analysis) procedure introduced by Vaz and Silvestro (2014). This technique is used to derive the main trends of the ripples, providing information about wind/sediment interactions at smaller scales (Figure 3).

The lee fronts of the dune slip faces were manually digitized on the S1 and T3 images in order to derive the dune migration rate and direction (Figure 4). In addition, we also evaluated the spatial distribution of the dune migration azimuth (Figure 5). We then used COSI-Corr to track the ripple displacement over the S1 and T3 images acquired 1359 Earth-days apart (Table 1). The result is a ripple displacement map (Figure 6) from which we derived the average ripple migration rate (Figures 7 and 8).

Finally, we estimated the potential timing of the sand-moving events by using the MRAMS mesoscale atmospheric model (Michaels and Rafkin, 2008; Rafkin et al., 2001) on two diverse grid scales. In the first one, the surface stress and wind direction have been modeled for one typical day for each of the four seasons (at L_s = 210° (southern summer), L_s = 300° (southern spring), L_s = 30° (southern winter) and L_s = 120° (southern autumn) at a spatial resolution of ~8 km x 8 km (Figure

9). The output model state was recorded every twenty Martian-minutes for four typical sols.

In the second atmospheric simulation, we used a model with ~2km grid spacing to constrain the local wind conditions in the Herschel Crater (Fig.10). The modeled winds have been sorted into 24 equal width direction bins over the dune field and each point may have a maximum 24 vectors and these ones show the downwind direction of the wind.

The instantaneous model was recorded for 12 seasons at Ls=0°(southern winter), Ls=30°(southern winter), Ls=60°(winter), Ls=90°(northern winter), Ls=120°(southern autumn), Ls=150°(autumn), Ls=180°(northern autumn), Ls=210°(southern summer), Ls=240°(summer), Ls=270°(northern summer), Ls=300°(southern spring) and Ls=330°(spring) by the MRAMS (Fig.11).

3. Dune and ripple morphology

The study dunes are located in a ~1200 km^2 dune field in the western floor of Herschel crater and consist of barchans and barchanoids (Cardinale et al., 2012b). These dunes can be more than 60 m tall and spaced ~200-800 m apart. Some of the dunes present an asymmetric structure, with the slip face being elongated obliquely (Figures 2b and c). Visual assessment and stereonet analysis reveal a high dispersion in the dune slipface orientation and slope values clustering at ~30° (Figure 2d). This reflects the concave shape of the barchan and barchanoid slipfaces. Most of the slip face vectors are oriented toward the south, trending between ~60° and ~300° with a main mode located at ~125° (Figure 2d), reflecting the dune slipface asymmetry.

In Figure 3 we show some examples of the different types of ripple patterns in the area. On the dune flanks ripples are spaced 2-4 meters apart and are two-dimensional with typical “Y” junction terminations (Figure 3a), while on the top of the dunes the ripple pattern is more three-dimensional, with diverse ripple sets overlapping (Figure 3b). Such a ripple arrangement probably reflects the coupling between ripple straightness and slope described by Rubin (2012) and observed in the field by Howard (1977). The complexity of the ripple pattern is shown in the rose diagram in Figure 3c (showing the distribution of the crestline trends mapped automatically over the dunes in the yellow box). The overall length-weighted circular distribution of the mapped ripple traces shows different trends and two main modes at ~45º and ~135º.

4. Bedform migration

4.1. Dunes

In Figure 4a we show the areal distribution of the average dune migration vectors for 211 dunes computed by comparing the pair S1 and T3 (Table 1) (Δt= 1359 Earth-days). Dunes which do not have a clear slipface are excluded from the analysis. The distribution of the lee motion is neither uniform nor unidirectional. A higher migration value is reported for the dunes located in the northern dune field sector (1.2-2.2 (m)) with the dune displacements decreasing toward the south (Figure 4a). Such a N-S migration trend can be attributed to the abrupt change in the roughness at the dune field margin which triggers the development of an internal boundary layer that thickens downwind (Jerolmack et al., 2012). Figure 4b highlights the north-south migration trend (left) and shows that the area with larger migration values (between -14.70° and -14.75° in latitude) corresponds to a drop in elevation that is well represented in the northern part of the Herschel dune field (right). This suggests that the underlying large-scale topography also contributes to the shape of the internal boundary layer.

On average, the dunes migrated 0.8 meters toward the SSE (Figure 5a shows the computed average vector) giving a rate of migration of 0.45 meter/Mars-year (MY) (~0.2 meter/Earth-year or m/EY), assuming that this values is constant from year to year. The measurements show high directional dispersion (μ=162°±38°) (Figure 5b), which might be partially be due to the local topography since the dunes are not migrating over a flat surface.

4.2. Ripples

In Figure 6 we show the ripple displacement map obtained with COSI-Corr. The map reveals that significant movement occurred across the investigated area between March 2007 and December 2010. In the northern area of the Herschel dune field the fastest ripples moved so far that the correlation breaks down, that is, once the migration exceeds a distance at least equal to the ripple wavelength (5.1 m) (Figure 6b). In the central and southern dune field sectors the ripple displacement is smaller, so it can be traced (Figures 6a and c). The ripple migration rate also varies with the height of the dunes, with the fastest migrating ripples located close to the dune crest of the dunes (Figure 6c). This is the result of the linear relationship between height and ripple migration also reported for the Nili Patera dunes (Bridges et al., 2012). During a period of 1359 Earth-days we obtained an average vector for ripple migration of 1.1 meters and trending toward SSE (Figure 7a). This gives a migration rate of 0.55 meters in one MY (~ 0.3 meters/EY). The measurements show a high circular standard deviation (41.6°) and their directional trend is mainly bimodal with modes at ~175° and ~240° (Figure 7b). The high directional dispersion of the ripple migration vectors is due to the local dune topography which deflects the wind over the dunes as shown in Figure 8. In particular, the secondary mode at ~240° is due to the ripple migration vectors in the lee of the dunes (orange vectors in Figure 8).

5. Modeled winds

The atmospheric models (MRAMS simulations at 2 diverse grid scales) are used to valuate wind strength and direction, to explain the observed aeolian morphologies and dune changes (Fenton et al., 2005; Hayward et al.,2007; Chojnacki et al., 2011).

Due to the complex pattern of the Herschel dune field, we suppose a multi directional wind regime to be estimated by these simulations.

In Figures 9a and 9b (wind model at 8 km grid space) we show the daily maximum MRAMS ratio (stress / threshold stress) vectors over the whole dune field. We define the stress ratio as the aerodynamic surface stress divided by the minimum threshold aerodynamic stress calculated using the expressions of Greeley and Iversen (1985). Dominant modeled wind direction is from the west to the east (Figure 9c) with the strongest winds blowing close to the western crater rim (Figure 9a). The predicted stress values are just above the (Kok 2010) threshold for sand saltation maintenance (10% of the Greeley and Iversen (1985) saltation initiation threshold). In Figure 9b we show the modeled wind directional variability. A general trend is visible with the winds being more unidirectional close to the western crater rim (see the lower circular STD in this area and Table 2). In Figure 9d we show the same data plotted by seasons with the important statistic parameters summarized in Table 2.

The strongest winds blow at Ls=30° (southern winter) from the west to the east with a circular STD of 34°. In the other seasons modeled winds are weaker and multi-directional (CSTD>87°). Dominant winds from the north to the south, matching the dune and ripple migration direction, are not predicted by the model.

Output from MRAMS at 2km grid scale such as that of Fig. 10 is used to resolve topographically – influenced wind flows not explained in the previous wind simulation.

Modeled wind strength and direction from twelve Martian sols are examined here (Fig.11).

Within the investigated dune field a predominant wind distribution is not visible; a wind direction variability possibly induced by the crater topography is high in all the twelve studied seasons and the strongest modeled winds are predicted to blow from N-NE in spring (Ls=330°).

The modeled winds by this second MRAMS simulation highlights that prevailing winds from north, matching the measured slip faces, are not predicted by this model.

According to this second simulation, we noticed that weaker winds are frequent in the Herschel Crater such as other areas previously studied (Silvestro et. al.2012, 2013).

Even in this second model, the simulated shear stress values are just above the Kok threshold for sand saltation maintenance with a maximum stress value of 0.30 for all the investigated seasons (Fig.12).

According to the recent numerical models on the Martian sand saltation, the hypothesis on the hysteresis phenomenon could show how after the initiation, the saltation can be sustained with weaker winds on martian surface (Kok, 2010).

6. Discussion and conclusion

Our results show that the ripples and the dunes in the Herschel Crater are mainly shaped by winds blowing from the north to the south. However, the asymmetry in the dune form indicates that the wind regime is not strictly uni-directional (Bourke M.C., 2009; Parteli et al., 2014).

In particular, following the model of Bagnold, (Bagnold, 1956), the influence of a local bimodal wind regime (winds blowing from NNW and from NNE), should be the cause for the observed asymmetry with the former probably being more frequent or stronger (Figure 2b-c).

The influence of more than one wind, the combination of dune collision, limb extension and merging with downwind dunes (Bourke M.C., 2009) are also supported by the dunefield pattern which is highly irregular and intricate (Bridges et al., 2007) and by the resultant bedform migration directions.

The first MRAMS simulation, show modeled winds enhanced by the western crater rim blowing to the east. The interaction of these flows with the dominant winds coming from the north may be the cause of the observed dune morphology and migration direction. In the second MRAMS simulation, the diverse combined wind flows may partially explain the intricate ripple pattern. The ripple migration however, seems to be controlled by the local dune topography and any extrapolation from local to dune field/regional scale has to be treated carefully.

The lack of dominant winds from the north in the MRAMS simulation can be attributed to the low spatial and temporal coverage. A similar situation has also been reported by other workers (Hayward et al., 2009; Silvestro et al., 2012) suggesting the importance of ground truth data when deriving the wind regime of a certain area on Mars.

With the exception of the Nili Patera ripples, bedform migration rates in Herschel are comparable to other areas on Mars (Bridges et al., 2012; Silvestro et al., 2011, 2013). However, without continuous and long-term monitoring of Herschel and the other zones, this kind of inference remains speculative.

In flat areas, changes in surface roughness can increase the boundary shear stress in the upwind margins of dune fields (Jerolmack et al., 2012), producing spatial variations in the sediment fluxes. In more complex terrains, like in the floor of Herschel crater, the observed relationship between dune celerity and local topography (in particular the abrupt change in the roughness of ~1km illustrated in the Fig.4) suggests that in addition to the roughness of the aeolian pattern, the variations in the long wavelenght topography (Pelletier et al., 2014) control the Herschel dunefield properties.

Collectively, the combination of different methods of investigation helped to better decipher the wind regime in Herschel Crater. At the dune field scale, the main winds from the north combine with wind from the west enhanced by the western crater rim (the dune field is distant 28 km from the westerly crater rim). At the dune scale, the topography of the dunes and the substrate topography are controlling dune height, bedform migration rates and directions as described for the White Sand dune field in New Mexico by Pelletier et al., 2014. The topography at regional and local scale is indeed an important boundary condition that needs to be carefully addressed in order to extract the best wind information from remote sensing images.

Acknowledgements

M. Cardinale is supported by a grant from the ASI (Agenzia Spaziale Italiana).

References

Bagnold, R.A. 1941. The physics of blown sand and desert dunes. London: Methuen, 265 pp.

Bourke, M.C. 2009. Barchan dune asymmetry: Observations from Mars and Earth. 2010 Icarus 205 (2010) , 183-197. DOI: 10.1016/j.icarus.2009.08.023.

Bourke, M.C., Edgett, KS., Cantor, BA. 2008. Recent Aeolian dune change on Mars. Geomorph 94, 247–255. http://dx.doi.org/10.1016/j.geomorph.2007.05.012.

Bridges, N.T., P. E. Geissler, A.S. McEwen, B.J. Thomson, F.C. Chuang, K. E. Herkenhoff, L.P. Keszthelyi, and S. Martínez-Alonso. 2007. Windy Mars: A dynamic planet as seen by the HiRISE camera, Geophys. Res. Lett., 34, L23205, doi:10.1029/2007GL031445.

Bridges, N.T., Bourke, M.C., Geissler, P.E., Banks, M.E., Colon, C., Diniega, S., Golombek, M.P., Hansen, C.J., Mattson S., McEwen A.S., Mellon, M.T., Stantzos N., and Thomson B.J. 2011. Planet-wide sand motion on Mars. Geology, January 2012, v.40, p. 31-34, first published on November 14, 2011, doi:10.1130/G32373.1.

Bridges, N. T., Ayoub F., Avouac J.P., Leprince S., Lucas A., Mattson S. 2012. Earth-like sand fluxes on Mars. Nature. 2012 May 9;485(7398):339-42. doi:10.1038/nature11022.

Bridges, N., Geissler, P.E., Silvestro, S and M. Banks. 2013. Bedform Migration on Mars: Current Results and Future Plans, Aeolian Research. http://dx.doi.org/10.1016/j.aeolia.2013.02.004.

Cardinale, M.; Silvestro, S.; Komatsu, G.; Vaz, D.A.; Michaels, TI. 2012a. Evidences for Sand Motion in the Equatorial Region of Mars. 43rd Lunar and Planetary Science Conference, 2012 LPI Contribution No. 1659, id.2452.

Cardinale, M., Komatsu, G., Silvestro, S. and Tirsch, D. 2012b. The influence of local topography for wind direction on Mars: two examples of dune fields in crater basins. Earth Surf. Process. Landforms, 37: 1437–1443. doi: 10.1002/esp.3289.

Chojnacki M., Burr D.M., Moersch J.E., Michaels T.I. 2011. Orbital observations of contemporary dune activity in Endeavour Crater, Meridiani Planum, Mars. Journal of Geophysical Research 116: E00F19, doi:10.1029/2010JE003675.

Fenton, L. K. 2006. Dune migration and slip face advancement in the Rabe Crater dune field, Mars, Geophys. Res. Lett., 33, L20201, doi:10.1029/2006GL027133.

Fenton, L.K., Toigo A.D., Richardson, M.I. 2005. Aeolian processes in Proctor Crater on Mars: mesoscale modelling on dune-forming winds. Journal of Geophysical Research 110: E06005. DOI: 10.1029/2004JE002309.

Geissler, P.E., Stantzos, N.W., Bridges, N.T., Bourke, M.C., Silvestro, S. and Fenton, L. K. 2013. Shifting sands on Mars: insights from tropical intra-crater dunes. Earth Surf. Process. Landforms, 38: 407–412. doi: 10.1002/esp.3331.

Greeley, R. & Iversen, J. D. 1985. Wind as a Geological Process on Earth, Mars, Venus and Titan. Cambridge Planetary Science Series no. 4. xii + 333 pp. Cambridge, London, New York, New Rochelle, Melbourne, Sydney: Cambridge University Press.

Hayward, R. K., Mullins, K. F, Fenton, L. K., Hare, T. M., Titus, T. N., Bourke, M. C., Colaprete A., Christensen. R. 2007. Mars Global Digital Dune Database and initial science results. Journal. Of Geophysical . Research,112, E11007, doi:10.1029/2007JE002943.

Hayward, R.K., Titus, T.N., Michaels, T.I., Fenton, L.K., Colaprete, A., and Christensen, P.R. 2009. Aeolian dunes as ground truth for atmospheric modeling on Mars: Journal of Geophysical Research, v. 114, E11012, doi:10.1029/2009JE003428.

Hansen, C.J., Bourke, M., Bridges, N.T., Byrne, S., Colon, C., Diniega, S., Dundas, C., Herkenhoff, K., McEwen, A., Mellon, M., Portyankina, G.,Thomas N. 2011. Seasonal Erosion and Restoration of Mars Northern Polar Dunes. Science 331: 575–578, doi: 10.1126/science.1197636.

Howard, H. D. 1977. Effect of slope on the threshold of motion and its application to orientation of wind ripples. Geological society of American Bulletin, 88: 853-856.

Kok, J.F. 2010. An improved parameterization of wind-blown sand flux on Mars that include the effect of hysteresis. Geophysical Research Letters, v.37, L12202, doi: 10.1029/2010GL043646.

Jerolmack, D.J. et al. 2012. Internal boundary layer model for the evolution of desert dune fields. Nature Geoscience 5, 206-209 (2012). doi:10.1038/ngeo1381.

Leprince S., Barbot S., Ayoub F.and Avouac J. P. 2007. Automatic and Precise Ortho-rectification, Coregistration, and Subpixel Correlation of Satellite Images, Application to Ground

Deformation Measurements, IEEE Transactions on Geoscience and Remote Sensing, Vol.45, No.6, June 2007.

Malin, M.C., Edgett, K.S. 2000. Sedimentary rocks of early Mars. Science, 290, 1927–1937, doi:10.1126/science.290.5498.1927, 8 December 2000.

Mattson, S., Kirk, R.L., Heyd, R., McEwen, A.S., Eliason, E., Hare, T., Beyer, R., Howington-Kraus, E., Okubo, C., and Herkenhoff, R.L. 2011. Release of HiRISE digital terrain models to the planetary data system: 42nd Lunar and Planetary Science Conference, The Woodlands, Texas: Lunar and Planetary Institute Contribution 1608, p. 1558.

Michaels, T.I., and Rafkin, S.C.R. 2008. Meteorological predictions for candidate 2007 Phoenix Mars Lander sites using the Mars Regional Atmospheric Modeling System (MRAMS): Journal of Geophysical Research, v. 113, E00A07, doi:10.1029/2007JE003013.

McEwen, A. S., et al. 2007. Mars Reconnaissance Orbiter's High Resolution Imaging Science Experiment (HiRISE), J. Geophys. Res., 112, E05S02, doi:10.1029/2005JE002605.

Parteli, E. J.R., Durán, O., Bourke, M. C., Tsoar, H., Pöschel, T., Herrmann, H. 2014. Origins of barchan dune asymmetry: Insights from numerical simulations, Aeolian Research, Volume 12, March 2014. Pages 121-133, ISSN 1875-9637, http://dx.doi.org/10.1016/j.aeolia.2013.12.002.

Pelletier, J. D. 2014. Controls on the large-scale spatial variations of dune-field properties in the barchanoid portion of White Sands dune field, New Mexico. Journal of Geophysical Research: Earth Surface. http://dx.doi.org/10.1002/2014JF003314.

Rafkin, S.C.R., Haberle, R.M., and Michaels, T.I. 2001. The Mars regional atmospheric modeling system: Model description and selected simulations: Icarus, v. 151, p. 228–256, doi:10.1006/icar.2001.6605.

Rubin, D.M. 2012. A unifying model for planform straightness of ripples and dunes in air and water. In: Third International Planetary Dunes Workshop: Remote Sensing and Image Analysis of Planetary Dunes. Flagstaff, Arizona, abst. #7020.

Silvestro, S., Vaz, D.A., Fenton, L.K., Geissler P.E. 2011. Active eolian processes on Mars: A regional study in Arabia and Meridiani Terrae. G. Res. Lett., 38, L20201, doi: 10.1029/2011GL048955.

Silvestro, S., Fenton, L. K., Michaels, T. I., Valdez, A. and Ori, G. G. 2012. Interpretation of the complex dune morphology on Mars: dune activity, modelling and a terrestrial analogue. Earth Surf. Process. Landforms, 37: 1424–1436. doi: 10.1002/esp.3286

Silvestro, S.,. Vaz, D. A., Ewing, R.C., Rossi, A.P., Fenton, L.K., Michaels, T.I., Flahaut J., and Geissler, P.E. 2013. Pervasive aeolian activity along rover Curiosity's traverse in Gale Crater, Mars. Geology, 2013, doi:10.1130/G34162.1.

Sparavigna, Amelia Carolina. 2013. Edge-detection applied to moving sand dunes on Mars. *arXiv preprint arXiv:1308.5315*.

Vaz, D.A., Silvestro, S. 2012. An object based approach for the mapping and characterization of Mars ripples. In: The Third International Planetary Dunes Workshop: Remote Sensing and Image Analysis of Planetary Dunes, Vol. Abs #7019, Flagstaff, AZ, USA.

Vaz, D.A., Silvestro S. 2014. Mapping and characterization of small-scale aeolian structures on Mars: An example from the MSL landing site in Gale Crater. Icarus, Volume 230, 15 February 2014, Pages 151-161. Third Planetary Dunes Systems. http://dx.doi.org/10.1016/j.icarus.2013.08.007.

Supplemental table

1. S1-S2-T3 HiRISE acquisition parameters.
2. Statistical parameters of the modeled winds divided by seasons.

Captions

1. **a)** Details of the study area, showing the distribution of the large dark dune fields within

Herschel Crater (MOLA shaded topography with Themis daytime mosaic). **b)** A perspective view of the large dark dunes from HiRISE images PSP_002860_1650 and ESP_020384_1650. A shaded relief map from MOLA data (top), showing the location of Herschel Crater.

2. The Herschel Crater dune field (CTX image P05_002860_1650_XI_15S232W) slope map derived from High Resolution Imaging Science Experiment digital terrain models (DTMs). **b-c)** Barchan dunes with and without elongated horns in the northern and north-eastern area of the dune field. The slope map suggests the presence of a slipface with a trend of 62°-286°, denoting a predominant wind direction blowing from the northeast (HiRISE image PSP_002860_1650). **d)** The lower hemisphere equal-area density stereoplot for all the slipface surface vectors estimated from the HiRISE DTMs. The estimated dip angle is ~30°
3. **a)** This inset represents the ripple length-weighted circular distribution (the mapped area corresponds to the yellow window shown in Fig. 2). The mapped ripple population exhibits a bimodal trend with two main modes trending 45° and 135°. **b)** An inset of a horn of a dune, where along its flanks, the ripple crests are continuous and have a two dimensional pattern. **c)** The pattern of the ripples superposing the dune’s slopes is complex due to the diverse wind flows blowing over the dunes.
4. **a)** Average dune lee front migration vectors overlain on the DTM. The colored vectors represent the average displacement of the slipface lee fronts over three Earth-years (from March 2007 to December 2010). **b-c)** The plots represent the statistics computed using 500 m moving windows for the migration and elevation at the base of the slipfaces. Note the general decrease of the displacements when moving south, and the association of the area with larger migrations (between -14.7° and -14.75°) with a drop in elevation.
5. **a)** This rose diagram shows the distribution of lee side migration azimuth**. b)** This rose diagram shows the circular distribution of the lee side migration.
6. Ripple displacement map for the Herschel Crater dune field, derived from correlated

HiRISE images with high displacements shown with warmer colors. **b)** Fast ripples moved so much that the correlation breaks down causing the observed fuzzy pattern. **c)** Area in which the correlation starts to record the ripple migration.

7. Circular distribution of the migration vectors. **a)** Ripple migration mean vector**. b)** This rose diagram shows the circular distribution of all ripple migration vectors. The secondary mode at ~240° is due to the ripple migration vectors in the lee of the dunes (see Figure 8).
8. Daily maximum MRAMS stress (ratio) vectors computed from COSI-Corr vectors data.
9. MRAMS modeled wind stresses and directions. **a)** Daily maximum stress ratio vectors for each of the 36 model nodes covering the dune field. The azimuth of the vectors corresponds to the wind direction while the color is the ratio between the model aerodynamic surface stress and the aerodynamic stress threshold for saltation initiation (Greeley and Iversen, 1985**) b)** Circular standard deviation associated with the mean vectors shown in a). **c)** Circular distribution of the wind stress ratio vectors. **d)** Mean stress ratio vectors of the modeled winds divided by seasons.
10. MRAMS winds in a GIS format over the studied dune field during the 12 investigated seasons. Only winds >10%of the Greeley and Iversen saltation initiation threshold are included in this plot. Each vector shows the downwind direction of the wind (the direction of the wind is flowing toward). The length of each vector is proportional to the greatest sfc_stress/sfc_stress_treshold ratio at the point of the direction while the color shows the relative frequency of each wind direction at each point (warmer colors correspond to more winds blowing in that direction).
11. Each circular distribution contains the combined information of all 21 MRAMS higher resolution points within the outline of one of the studied HiRISE images (see Fig.10) . the radial direction in these plots is magnitude (of stress/stress_threshold), with the outer ring being a value of 0.3 and the center of each plot being 0. Each bin is colored by the relative frequency of each wind direction/magnitude (warmer colors correspond to more winds

blowing in that direction).

12. The circular distribution shows the sum of all the 12 investigated seasons.

Table1

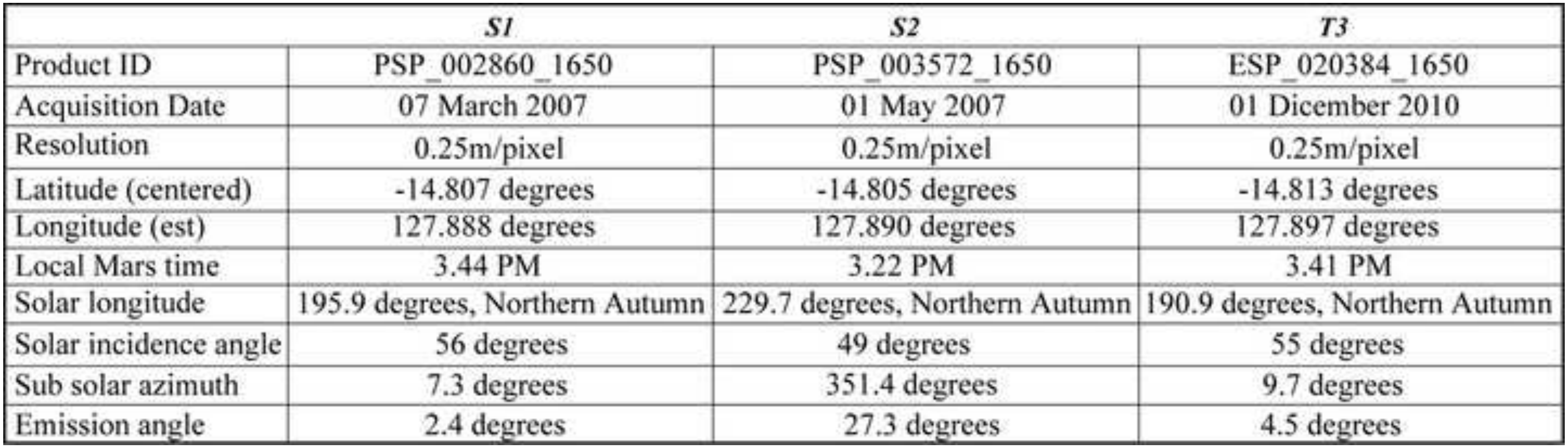

	S1	*S2*	*T3*
Product ID	PSP_002860_1650	PSP_003572_1650	ESP_020384_1650
Acquisition Date	07 March 2007	01 May 2007	01 Dicember 2010
Resolution	0.25m/pixel	0.25m/pixel	0.25m/pixel
Latitude (centered)	-14.807 degrees	-14.805 degrees	-14.813 degrees
Longitude (est)	127.888 degrees	127.890 degrees	127.897 degrees
Local Mars time	3.44 PM	3.22 PM	3.41 PM
Solar longitude	195.9 degrees, Northern Autumn	229.7 degrees, Northern Autumn	190.9 degrees, Northern Autumn
Solar incidence angle	56 degrees	49 degrees	55 degrees
Sub solar azimuth	7.3 degrees	351.4 degrees	9.7 degrees
Emission angle	2.4 degrees	27.3 degrees	4.5 degrees

Table2

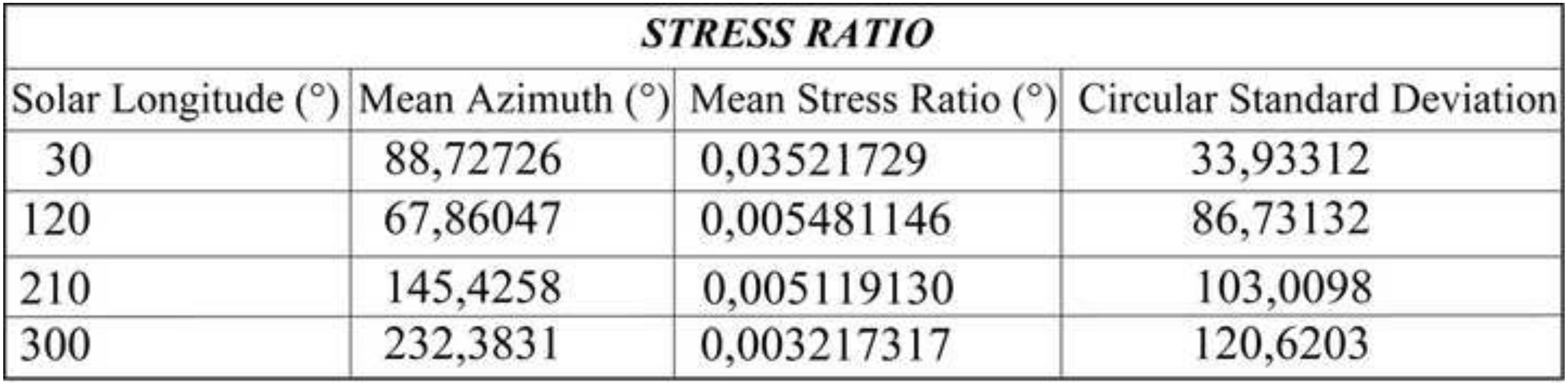

STRESS RATIO			
Solar Longitude (°)	Mean Azimuth (°)	Mean Stress Ratio (°)	Circular Standard Deviation
30	88,72726	0,03521729	33,93312
120	67,86047	0,005481146	86,73132
210	145,4258	0,005119130	103,0098
300	232,3831	0,003217317	120,6203

Figure1

Click here to download high resolution image

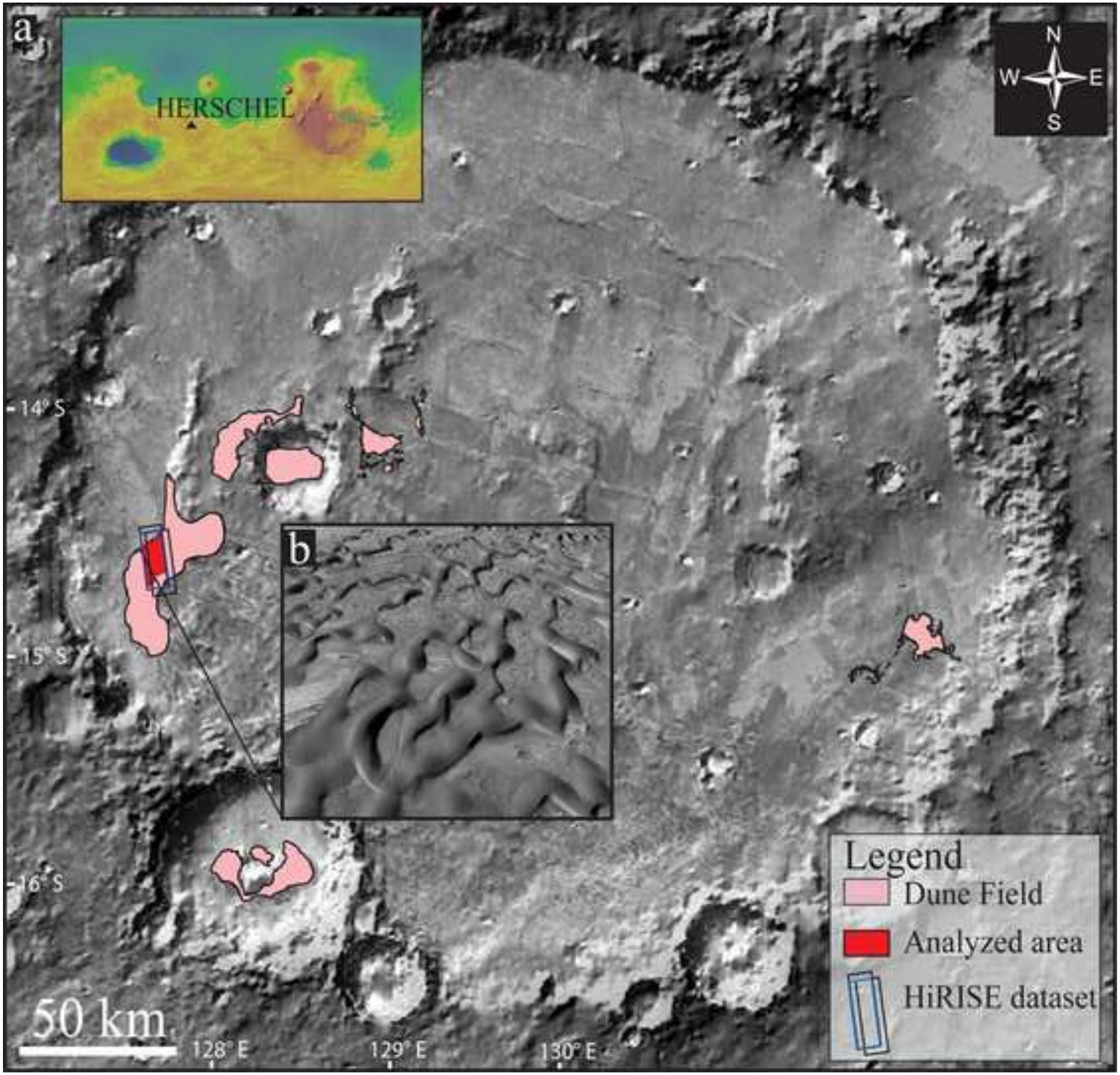

Figure2

Click here to download high resolution image

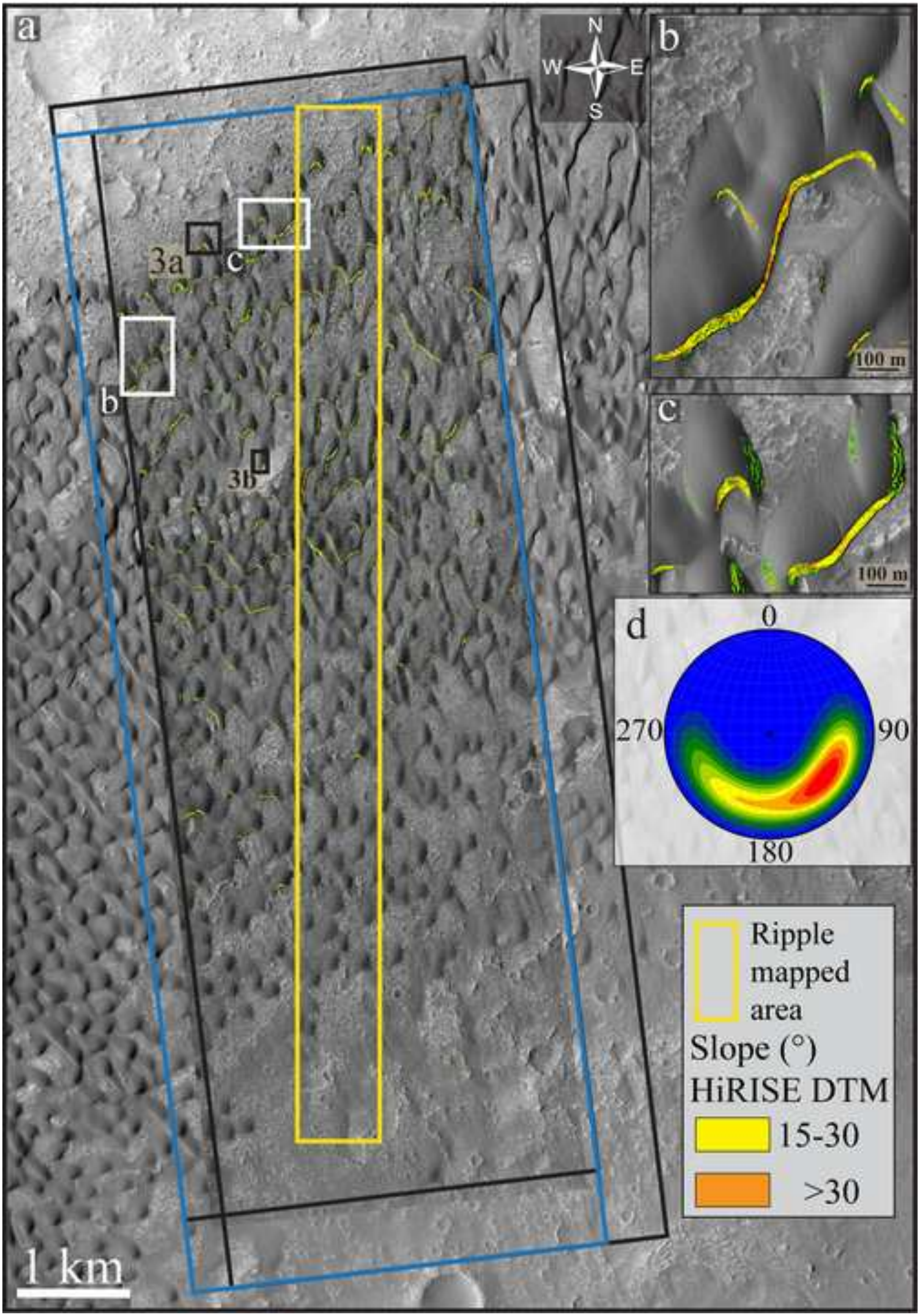

Figure3

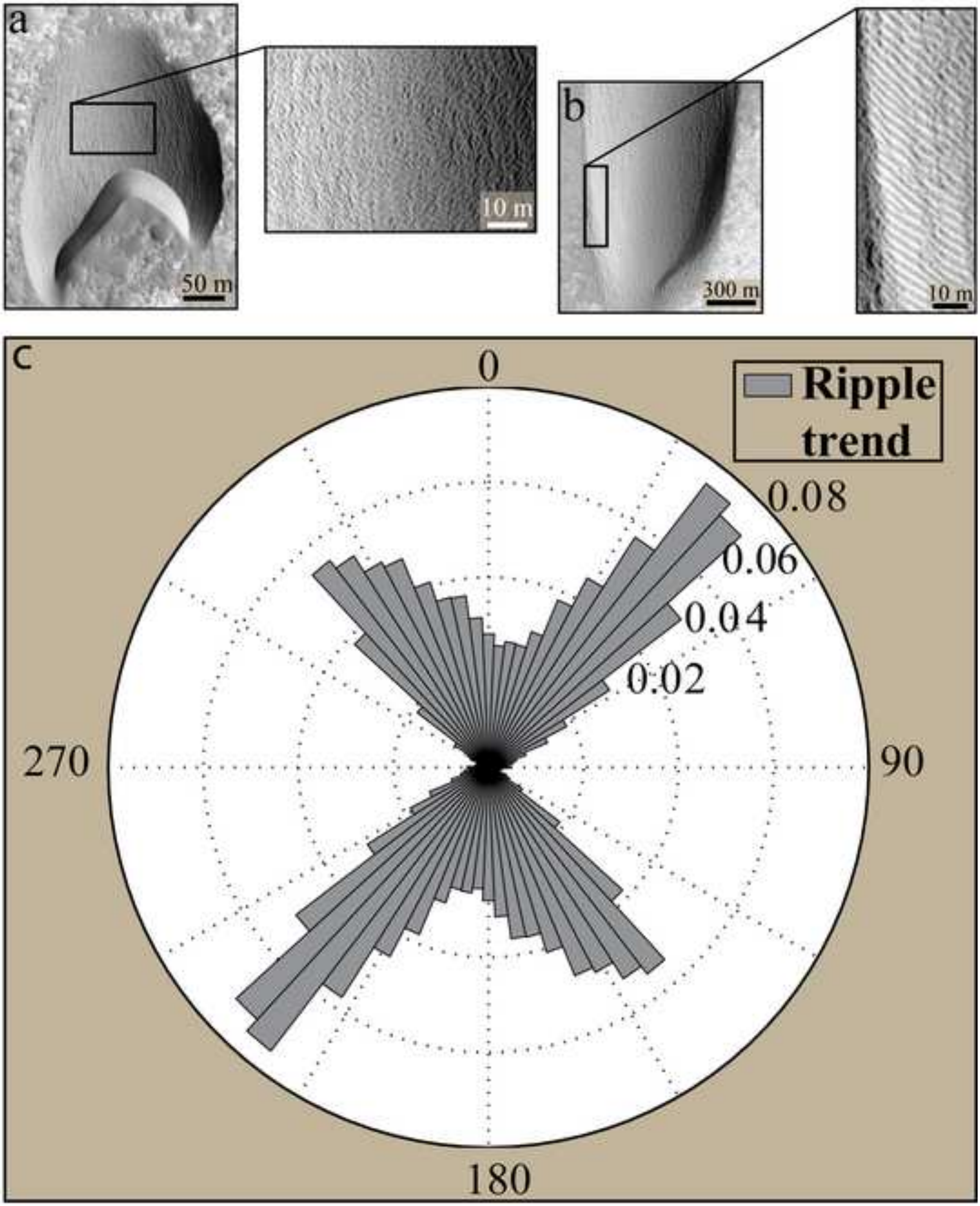

Figure4

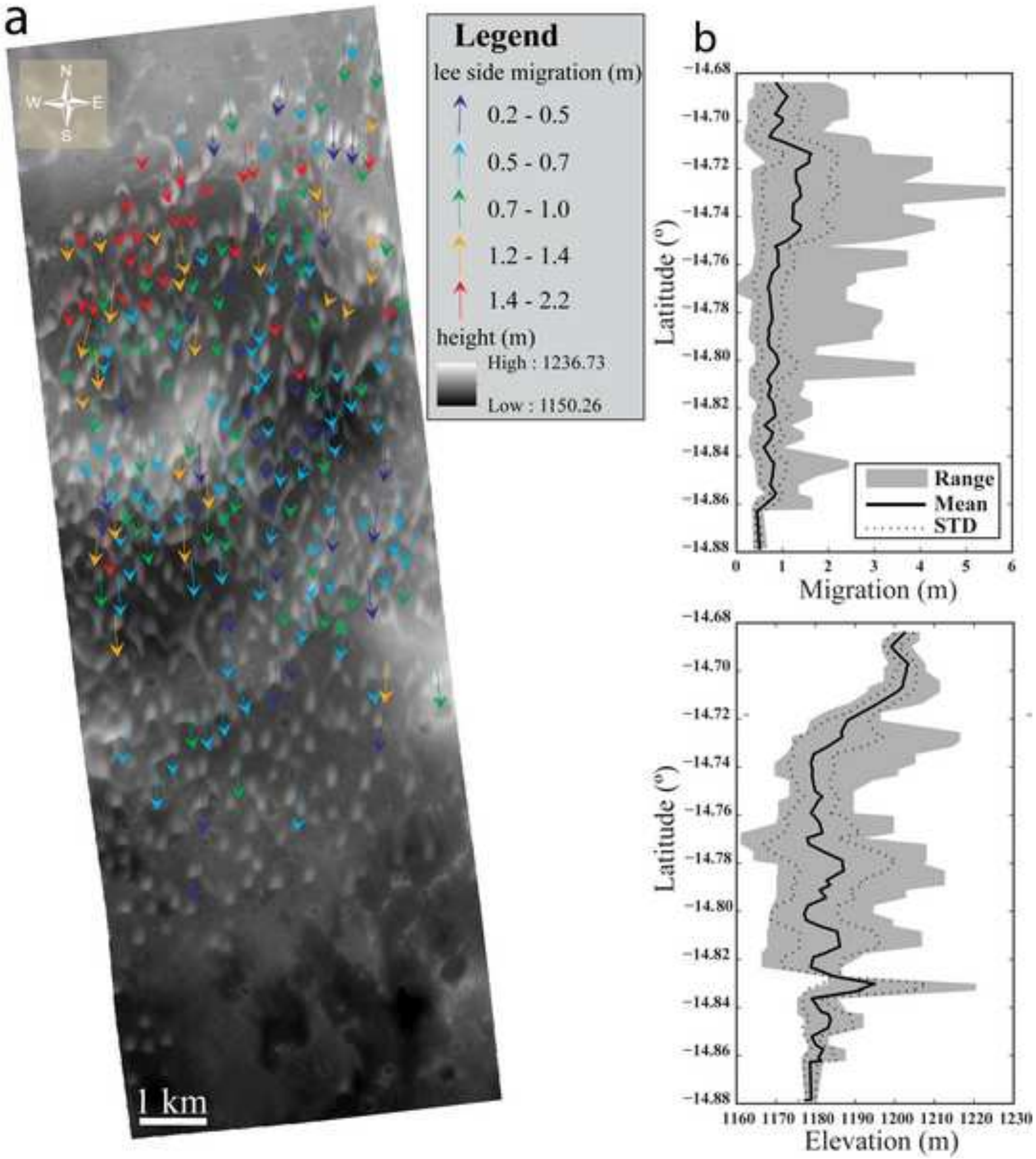
a
N
W
E
S
1 km
Legend
lee side migration (m)
0.2 - 0.5
0.5 - 0.7
0.7 - 1.0
1.2 - 1.4
1.4 - 2.2
height (m)
High : 1236.73
Low : 1150.26
b
Latitude (°)
-14.68
-14.70
-14.72
-14.74
-14.76
-14.78
-14.80
-14.82
-14.84
-14.86
-14.88
Range
Mean
STD
0
1
2
3
4
5
6
Migration (m)
1160
1170
1180
1190
1200
1210
1220
1230
Elevation (m)

Figure5

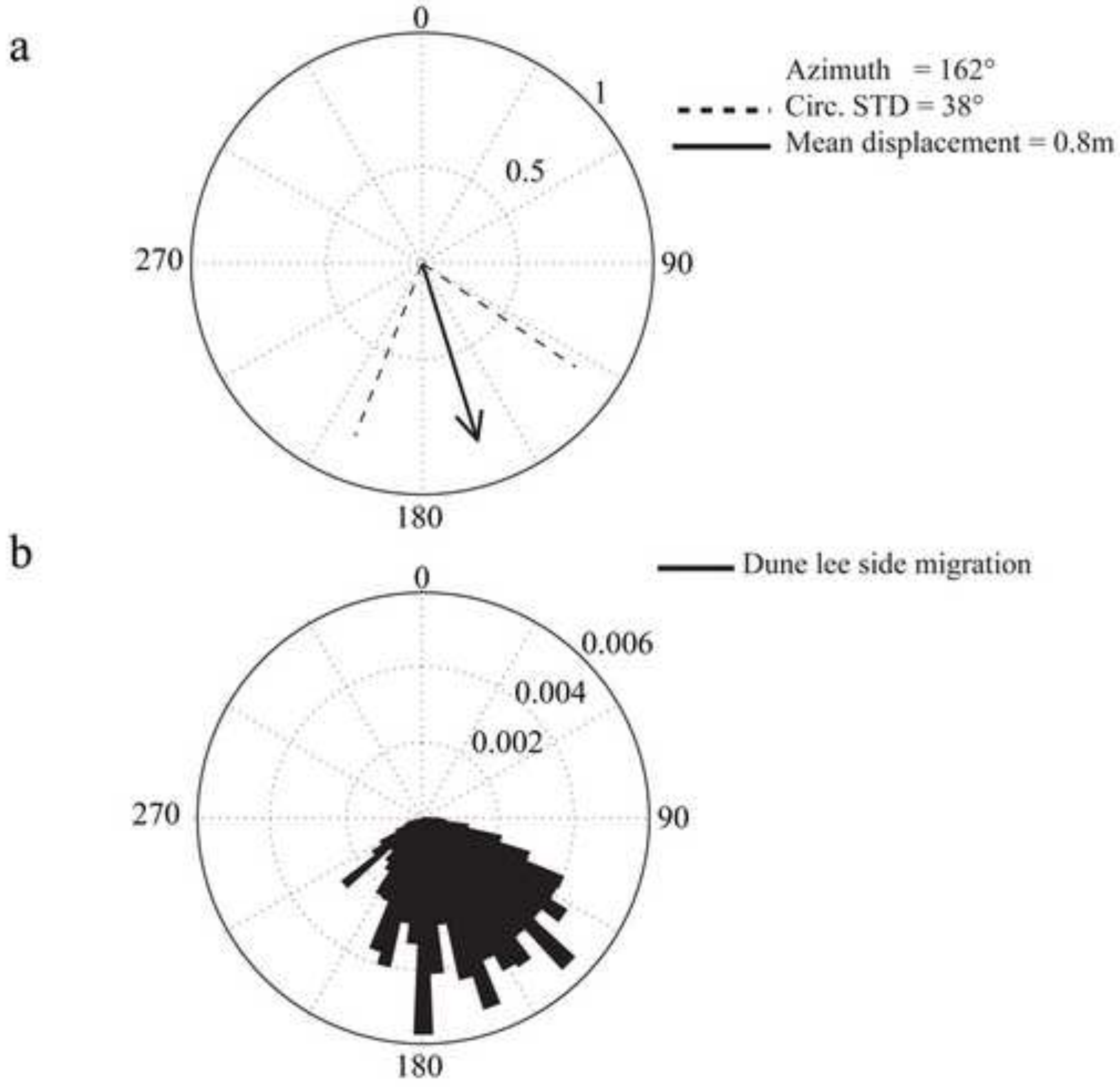
a
0
1
0.5
270
90
180
Azimuth = 162°
Circ. STD = 38°
Mean displacement = 0.8m
b
0
0.006
0.004
0.002
270
90
180
Dune lee side migration

Figure6

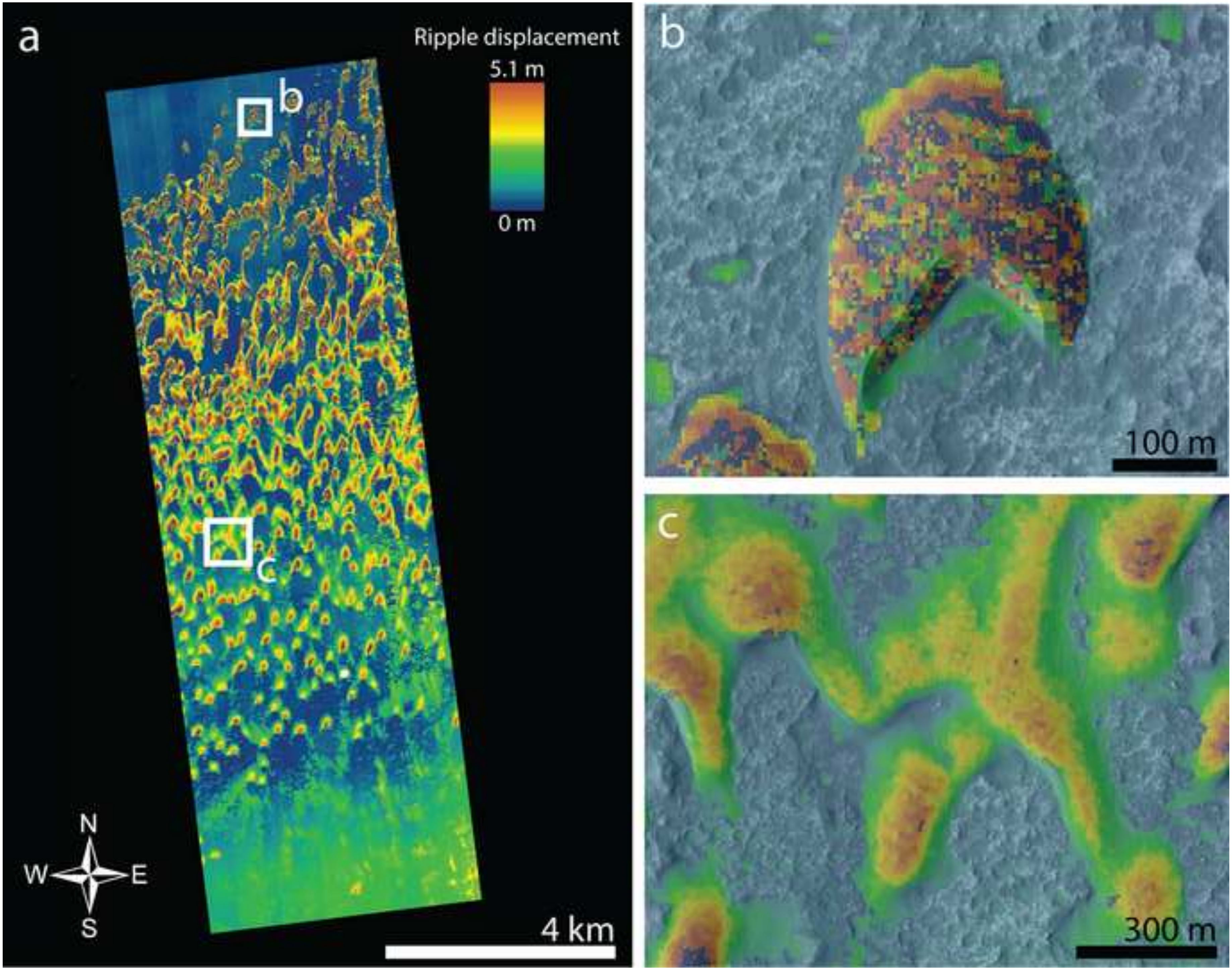

Figure7

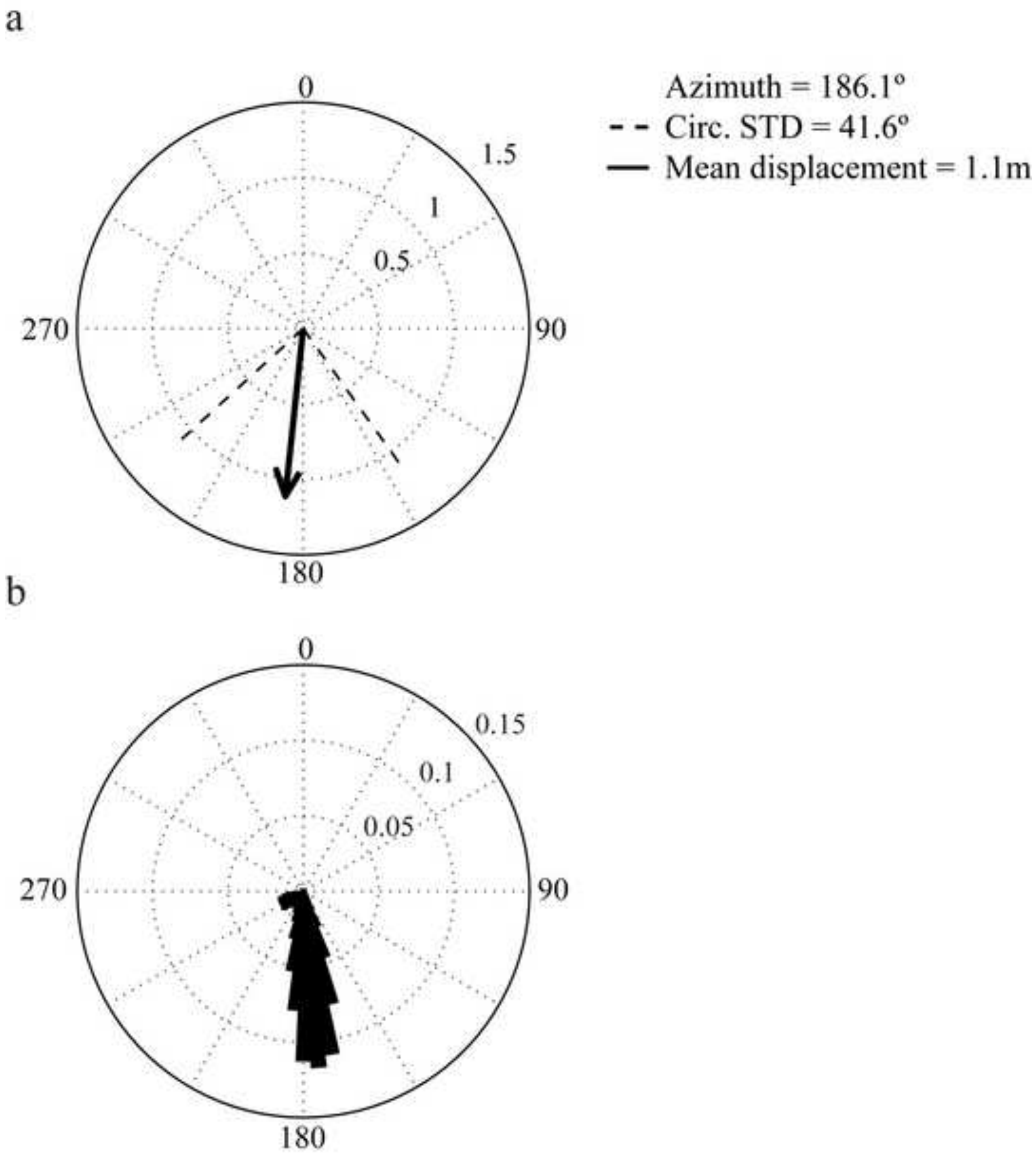
a
0
1.5
1
0.5
270
90
180
Azimuth = 186.1°
Circ. STD = 41.6°
Mean displacement = 1.1m
b
0
0.15
0.1
0.05
270
90
180

Figure8

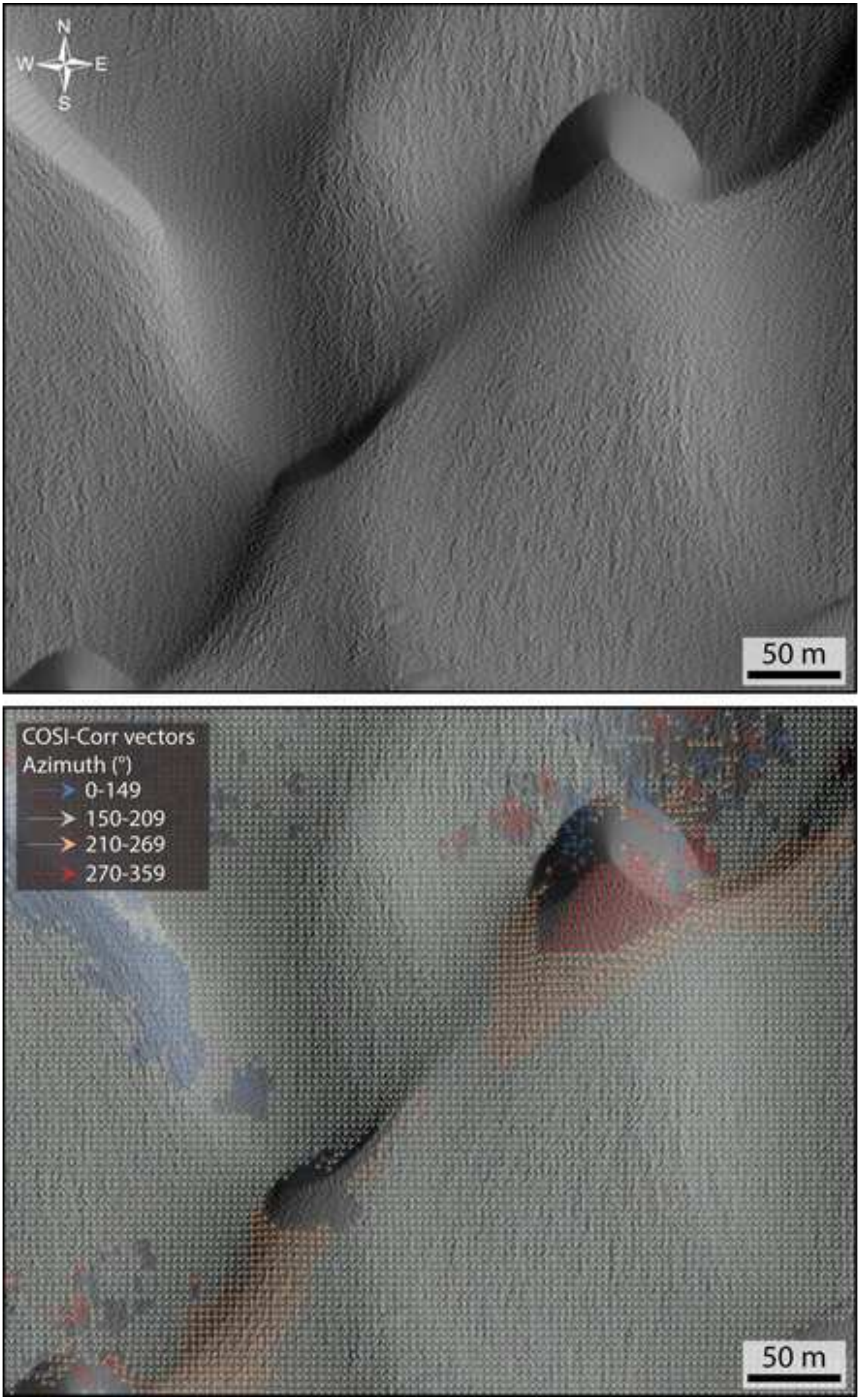
N
W
E
S
50 m
COSI-Corr vectors
Azimuth (°)
0-149
150-209
210-269
270-359
50 m

Figure9

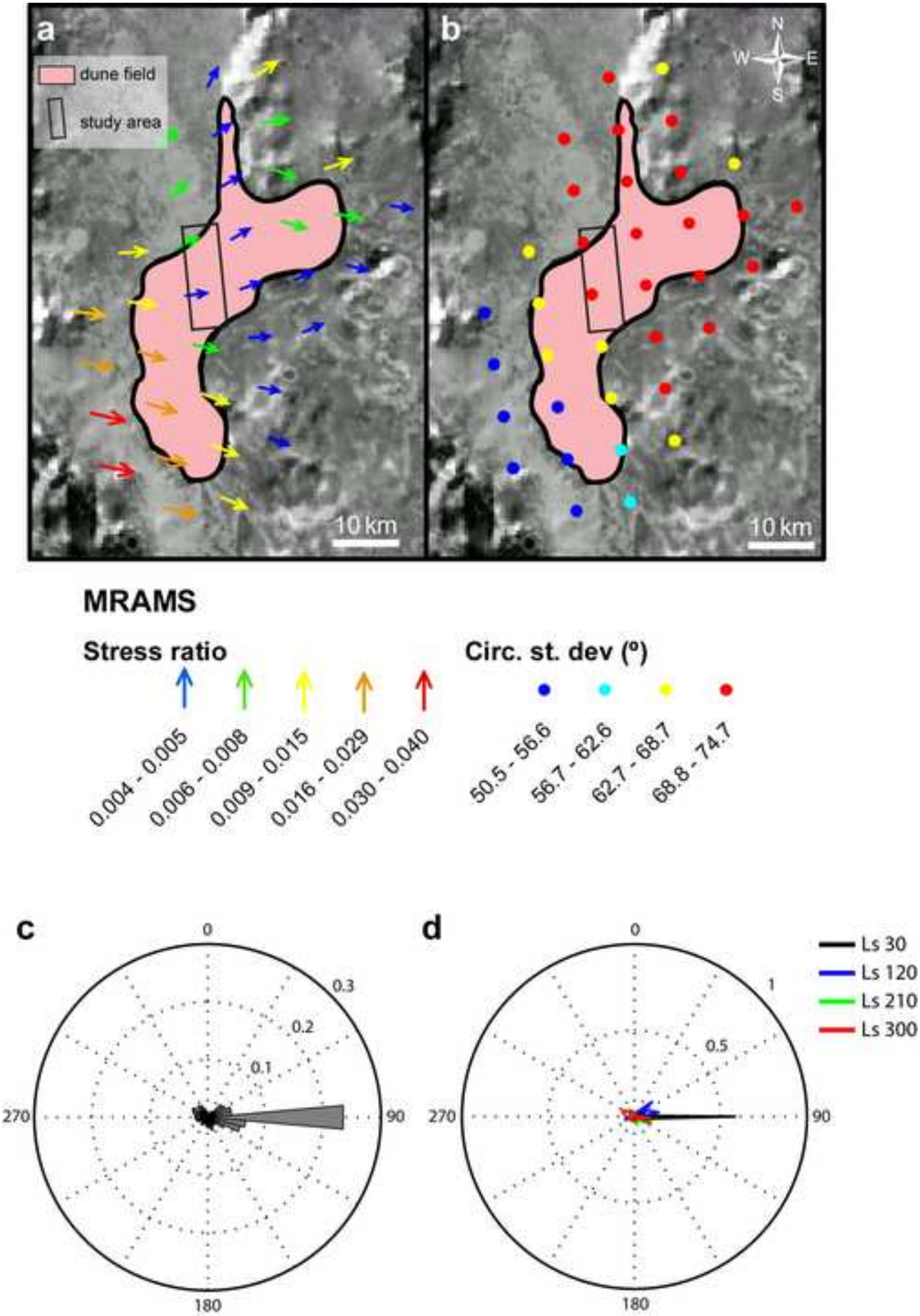
a
dune field
study area
10 km
b
N
W
E
S
10 km
MRAMS
Stress ratio
0.004 - 0.005
0.006 - 0.008
0.009 - 0.015
0.016 - 0.029
0.030 - 0.040
Circ. st. dev (º)
50.5 - 56.6
56.7 - 62.6
62.7 - 68.7
68.8 - 74.7
c
0
0.3
0.2
0.1
270
90
180
d
0
1
0.5
270
90
180
Ls 30
Ls 120
Ls 210
Ls 300

Figure10

Click here to download high resolution image

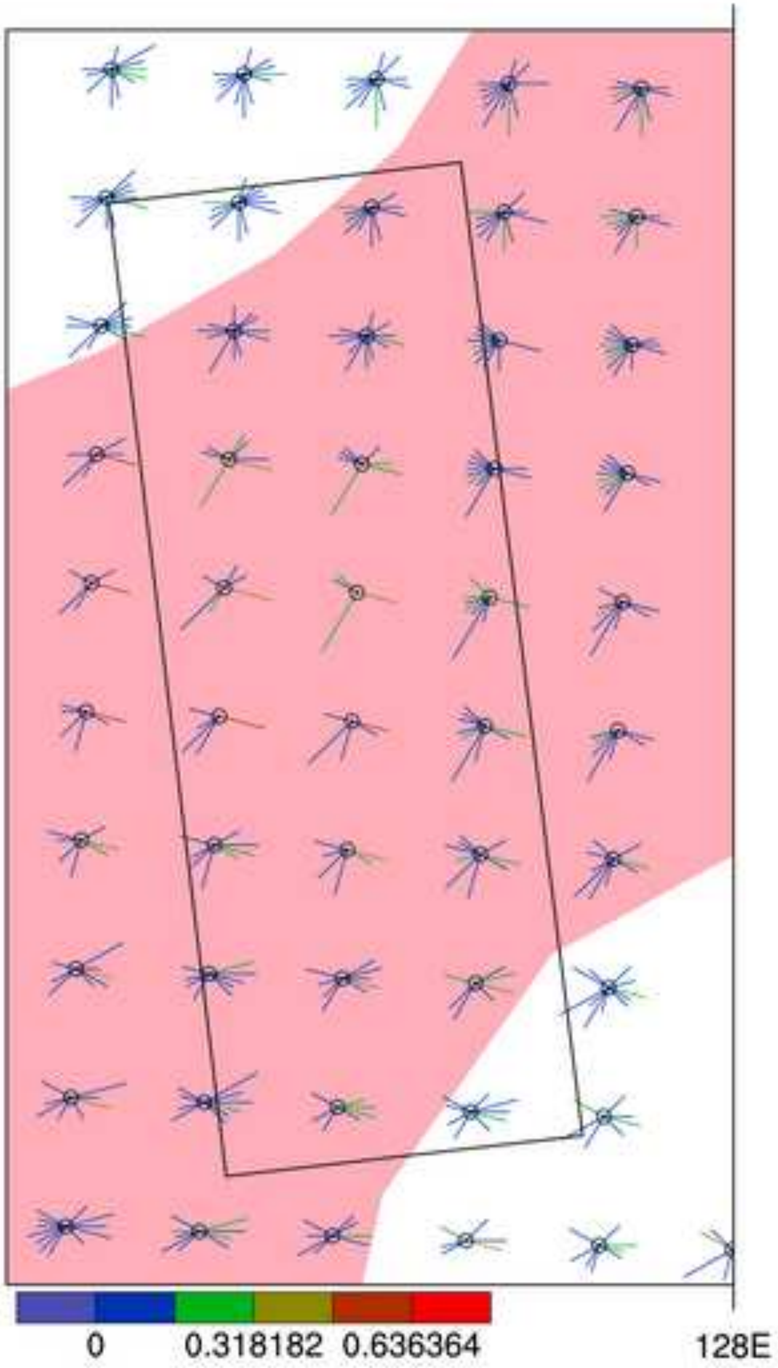

Figure11

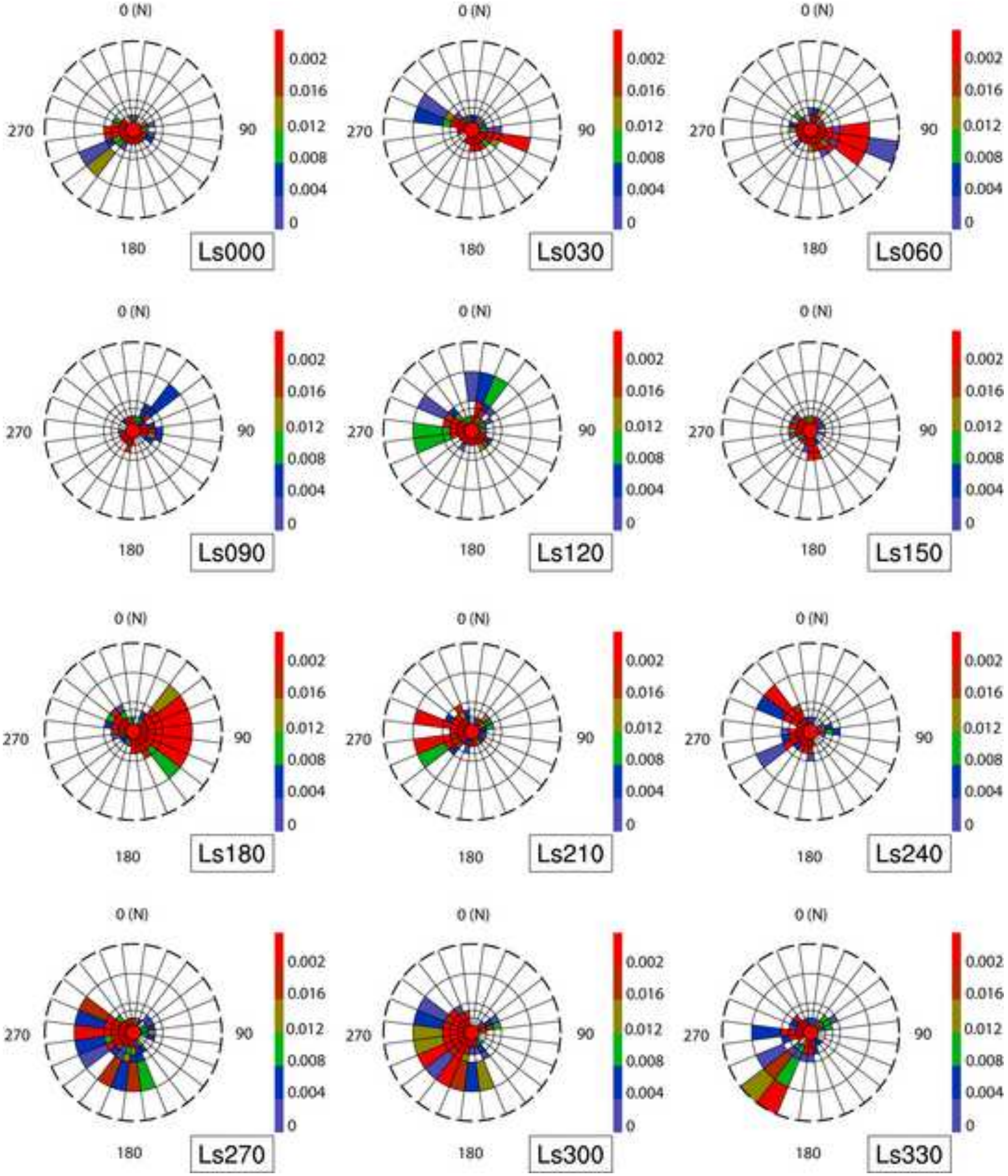
0 (N)
270
90
180
0.002
0.016
0.012
0.008
0.004
0
Ls000
Ls030
Ls060
Ls090
Ls120
Ls150
Ls180
Ls210
Ls240
Ls270
Ls300
Ls330

Figure12